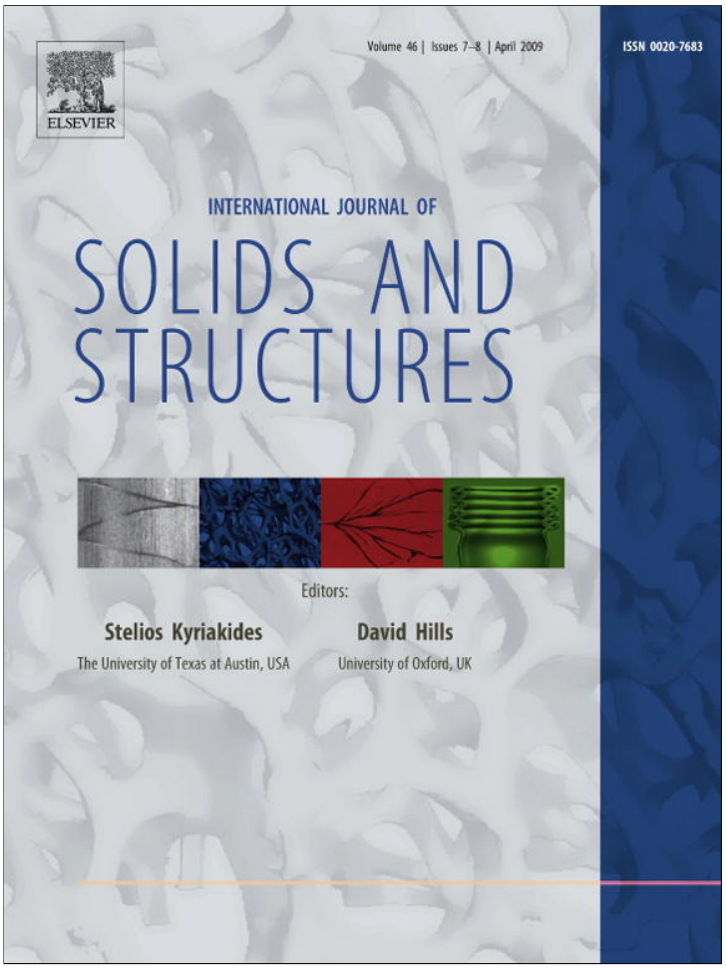

International Journal of Solids and Structures 46 (2009) 1764–1771

Contents lists available at ScienceDirect

International Journal of Solids and Structures

journal homepage: www.elsevier.com/locate/ijsolstr

Nonlinear analysis of elastic high-shear deformable plane frames by a mixed FEM path-following approach

Antonio D. Lanzo *

Universitá della Basilicata, DiSGG (Dip. Strutture, Geotecnica e Geol. Appl.), Campus Macchia Romana, 87100 Potenza, Italy

ARTICLE INFO

Article history:
Received 18 September 2008
Received in revised form 16 December 2008
Available online 14 January 2009

Keywords:
Nonlinear elasticity
Cosserat beam model
Finite element
Path-following analysis
Mixed formulation

ABSTRACT

This paper deals with the nonlinear analysis of high-shear deformable elastic plane frame, frequently used to model beam of composite materials, elastomeric beam-like bearings of bridge and seismic isolation, or to model DNA strands and polymer chains. The work uses a FEM approach based on a Cosserat–Timoshenko beam model with an exact geometrical description, evaluating all the axial, shear and bending contributions. It follows a mixed implementation of a Riks-path following locking-free strategy of analysis, exploring its implementation details and proving its effectiveness and reliability. At last the paper reports the quantitative and qualitative influence of shear contribution on known classical examples.

1. Introduction

FEM analysis of geometrically nonlinear elastic plane frame is a topic widely discussed in literature, either using Riks standard path-following arch-length strategies (Riks, 1972, 1979) or Koiter perturbative approaches (Salerno and Lanzo, 1997). A hypothesis that is widely accepted in the relevant literature is that of representing beam structural elements taking into account only their flexural and, sometimes, axial deformation effects, while nearly always neglecting their shear deformation contributions. Nevertheless, situations can be found that do not fit this hypothesis, where shear deformation effects are not negligible and fundamental to the analysis. For instance, the analysis of beam of composite materials and elastomeric beam-like bearings (frequently used in bridge and seismic isolation), or the modeling of DNA strands and polymer chains, etc. This work aims to take into account these situations.

While a previous paper (Lanzo, 2004) focuses on the beam model in a perturbation strategy of analysis, the present paper aims to examine aspects connected to the use of a path-following numerical reconstruction strategy of the equilibrium path. In this respect, the work follows a mixed variant of the classical arch-length method of Riks, initially suggested in Garcea et al. (1998) as a solution of some locking problems, using a step control defined both in terms of displacements and internal stress components, in addition to the load parameter. In the present paper, the internal stress component referred to are the axial and the transversal tension components (N, T) of the beam elements, and not merely the axial component N as considered in the paper by Garcea et al. (1998), where the shear effects are substantially neglected. In this study a geometrically exact Cosserat–Timoshenko beam model (Rubin, 2000) and an accurate discrete interpolation (exact in terms of stress components) are used.

The mixed path-following strategy suggested in the present paper proves to be reliable and numerically stable. A careful implementation also involves computational costs comparable to that of a traditional displacement-based path-following strategy.

2. The elastic beam model

A Cosserat–Timoshenko planar beam model (Rubin, 2000) is kinematically defined in terms of displacements components $(u[s], w[s])$ of the centroid axis in the problem plane (x, z)

$$\mathbf{p_o}[s] = (s + u[s])\mathbf{i} + w[s]\mathbf{k}$$

and in term of the rigid rotation $\varphi[s]$ of its generic section, with reference to an initial configuration with rectilinear axis of length l and sections orthogonal to it (see Fig. 1).

The strain allowed by the kinematical model includes axial, shear and bending deformations. For finite displacements, exact strain measures $(\varepsilon[s], \gamma[s], \chi[s])$ are defined by the relations (see Antman, 1977, 1995; Pignataro et al., 1982; Lanzo, 1994; Salerno and Lanzo, 1997)

$$\mathbf{r}_{,s} = (1 + \varepsilon)\mathbf{a} + \gamma\mathbf{b}, \quad \chi = \theta_{,s}$$

where $(\cdot)_{,s}$ stand for derivation with respect to the abscissa s and the unit vectors

* Tel.: +39 0971 205055; fax: +39 0971 205070.
E-mail address: antonio.lanzo@unibas.it

0020-7683/$ - see front matter © 2009 Elsevier Ltd. All rights reserved.
doi:10.1016/j.ijsolstr.2008.12.019

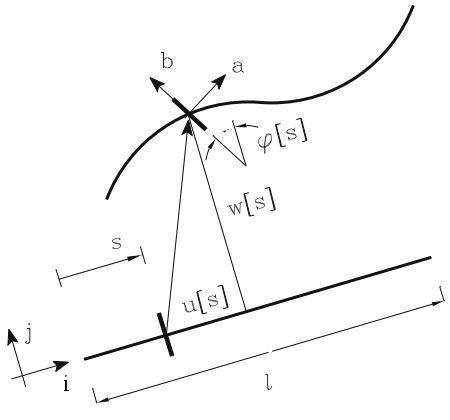

Fig. 1. Kinematic of Cosserat beam model.

$$\mathbf{a} = \cos\theta\ \mathbf{i} - \sin\theta\ \mathbf{k}, \quad \mathbf{b} = \sin\theta\ \mathbf{i} + \cos\theta\ \mathbf{k}$$

are, respectively, normal and tangent to the plane of the section in the deformed configuration. The development of the above definitions leads to the following nonlinear strain–displacement relationship

$$1 + \varepsilon = (1 + u_{,s})\cos\theta - w_{,s}\sin\theta \tag{1a}$$
$$\gamma = (1 + u_{,s})\sin\theta + w_{,s}\cos\theta \tag{1b}$$
$$\chi = \theta_{,s} \tag{1c}$$

Let (N, T, M) be force measures so that internal forces and couples of contact action are represented by the vectors

$$\mathbf{t} = N\mathbf{a} + T\mathbf{b}, \quad \mathbf{m} = M\mathbf{b} \times \mathbf{a}$$

In the absence of loads along the axis of the beam, the internal equilibrium conditions are the following

$$\mathbf{t}_{,s} = 0 \tag{2a}$$
$$\mathbf{m}_{,s} + \mathbf{r}_{,s} \times \mathbf{t} = 0 \tag{2b}$$

A simple linear elastic beam model is obtained by means of the following constitutive relations

$$N = k_n\varepsilon, \quad T = k_t\gamma, \quad M = k_m\chi$$

where k_n, k_t ed k_m are, respectively, the axial, shear and flexural stiffness moduli, from now on referred to as *EA*, *GA* ed *EJ*, for similarity with the classical linear beam model, i.e.

$$N = EA\varepsilon, \quad T = GA\gamma, \quad M = EJ\chi$$

3. A mixed formulation of the problem

A mixed formulation of the beam model can be obtained by setting its normal and shear internal stress components (N, T) as the primary variables of the problem, in addition to the displacement variables, and defining its internal strain energy by the following functional

$$\Phi[u, \boldsymbol{\sigma}] = \int_0^l \left\{ \boldsymbol{\sigma}^t \boldsymbol{\epsilon}_u - \frac{1}{2}\boldsymbol{\sigma}^t \mathscr{F}\boldsymbol{\sigma} + \frac{1}{2}EJ\chi^2 \right\} ds$$

where

$$\boldsymbol{\epsilon}_u = \begin{bmatrix} \varepsilon \\ \gamma \end{bmatrix}, \quad \boldsymbol{\sigma} = \begin{bmatrix} N \\ T \end{bmatrix}, \quad \mathscr{F} = \begin{bmatrix} \frac{1}{EA} & 0 \\ 0 & \frac{1}{GA^*} \end{bmatrix}$$

Alternatively, a more convenient mixed formulation can be obtained by referring instead to the new set of static variables $(\widetilde{N}, \widetilde{T})$ defined by

$$\mathbf{t} = \widetilde{N}\mathbf{i} + \widetilde{T}\mathbf{j}, \quad \underbrace{\begin{bmatrix} \widetilde{N} \\ \widetilde{T} \end{bmatrix}}_{\tilde{\boldsymbol{\sigma}}} = \underbrace{\begin{bmatrix} +\cos\varphi & -\sin\varphi \\ +\sin\varphi & +\cos\varphi \end{bmatrix}}_{\mathbf{R}^t_\varphi} \underbrace{\begin{bmatrix} N \\ T \end{bmatrix}}_{\boldsymbol{\sigma}}$$

In fact, because of the internal equilibrium conditions (2a), these new tension parameters $\tilde{\boldsymbol{\sigma}} \equiv (\widetilde{N}, \widetilde{T})$ are constant along the generic beam

$$\widetilde{N}_{,s} = 0, \quad \widetilde{T}_{,s} = 0$$

and then trivially represented in a FEM discrete approach. The internal strain energy can be rewritten in the new set of variables $r \equiv (u, \tilde{\boldsymbol{\sigma}})$ as

$$\Phi[u, \tilde{\boldsymbol{\sigma}}] = \int_0^l \left\{ \tilde{\boldsymbol{\sigma}}^t \tilde{\boldsymbol{\epsilon}}_u - \frac{1}{2}\tilde{\boldsymbol{\sigma}}^t \mathbf{R}^t_\varphi \mathscr{F} \mathbf{R}_\varphi \tilde{\boldsymbol{\sigma}} + \frac{1}{2}EJ\chi_u^2 \right\} ds$$

with

$$\tilde{\boldsymbol{\epsilon}}_u = \begin{bmatrix} \tilde{\varepsilon} \\ \tilde{\gamma} \end{bmatrix} = \mathbf{R}^t_\varphi \boldsymbol{\epsilon}_u \Longleftrightarrow \begin{cases} \tilde{\varepsilon}_u = 1 + u' - \cos\varphi \\ \tilde{\gamma}_u = w\prime - \sin\varphi \end{cases}$$

4. The variations of the strain energy

In order to develop a path-following analysis strategy, the first and second variations of the strain energy of the beam model are needed. The relative expressions follow

$$\begin{aligned} \Phi'\delta r = \int_0^l \Big\{ & \delta\tilde{\boldsymbol{\sigma}}^t \left(\tilde{\boldsymbol{\epsilon}}_u - \mathbf{R}^t_\varphi \mathscr{F} \mathbf{R}_\varphi \tilde{\boldsymbol{\sigma}} \right) + \tilde{\boldsymbol{\sigma}}^t (\tilde{\varepsilon}'_u \delta u) \\ & - \frac{1}{2}\delta\varphi \tilde{\boldsymbol{\sigma}}^t (\mathbf{R}'^t_\varphi \mathscr{F} \mathbf{R}_\varphi + \mathbf{R}^t_\varphi \mathscr{F} \mathbf{R}'_\varphi) \tilde{\boldsymbol{\sigma}} + EJ\varphi'\delta\varphi' \Big\} ds \\ \Phi''\dot{r}\delta r = \int_0^l \Big\{ & \delta\tilde{\boldsymbol{\sigma}}^t (\varepsilon'_u \dot{u}) + \dot{\tilde{\boldsymbol{\sigma}}}^t (\varepsilon'_u \delta u) + \tilde{\boldsymbol{\sigma}}^t (\varepsilon''_u \dot{u} \delta u) - \delta\tilde{\boldsymbol{\sigma}}^t \mathbf{R}^t_\varphi \mathscr{F} \mathbf{R}_\varphi \dot{\tilde{\boldsymbol{\sigma}}} \\ & - (\dot{\varphi}\delta\tilde{\boldsymbol{\sigma}} + \delta\varphi\dot{\tilde{\boldsymbol{\sigma}}})^t (\mathbf{R}'^t_\varphi \mathscr{F} \mathbf{R}_\varphi + \mathbf{R}^t_\varphi \mathscr{F} \mathbf{R}'_\varphi) \tilde{\boldsymbol{\sigma}} \\ & + \dot{\varphi}\delta\varphi \tilde{\boldsymbol{\sigma}}^t (\mathbf{R}^t_\varphi \mathscr{F} \mathbf{R}_\varphi - \mathbf{R}'^t_\varphi \mathscr{F} \mathbf{R}'_\varphi) \tilde{\boldsymbol{\sigma}} + EJ\dot{\varphi}'\delta\varphi' \Big\} ds \end{aligned}$$

In a FEM approach, the values of the rotation $\varphi[s]$ can be made small enough using an adequate discretization mesh. This allows the simplifications

$$\sin\varphi \approx \varphi, \quad \cos\varphi \approx 1 \tag{3}$$

By setting $k = \frac{1}{EA} - \frac{1}{GA}$, we therefore obtain the following simplified expression of the strain energy variations

$$\begin{aligned} \Phi'\delta r \approx \int_0^l \{ & \delta\widetilde{N}\left(u' - \frac{1}{EA}\widetilde{N} - k\varphi\widetilde{T} \right) \\ & + \delta\widetilde{T}\left(w' - \varphi - \frac{1}{GA}\widetilde{T} - k\varphi\widetilde{N} \right) + \delta u'\widetilde{N} + \delta w'\widetilde{T} \\ & + \delta\varphi\left(\widetilde{N}\varphi - \widetilde{T} + k\varphi(\widetilde{N}^2 - \widetilde{T}^2) - k\widetilde{N}\widetilde{T} \right)) + EJ\varphi'\delta\varphi' \} ds \\ \Phi''\dot{r}\delta r \approx \int_0^l \{ & \delta\widetilde{N}\dot{u}' + \delta\widetilde{T}\dot{w}' + \dot{\widetilde{N}}\delta u' + \dot{\widetilde{T}}\delta w' \\ & - \frac{1}{EA}\delta\widetilde{N}\dot{\widetilde{N}} - \frac{1}{GA}\delta\widetilde{T}\dot{\widetilde{T}} - k\varphi(\delta\widetilde{N}\dot{\widetilde{T}} + \delta\widetilde{T}\dot{\widetilde{N}}) \\ & + (\dot{\varphi}\delta\widetilde{N} + \delta\varphi\dot{\widetilde{N}})(\varphi + 2k\varphi\widetilde{N} - k\widetilde{T}) \\ & + (\dot{\varphi}\delta\widetilde{T} + \delta\varphi\dot{\widetilde{T}})(-1 - k\widetilde{N} - 2k\varphi\widetilde{T}) \\ & + \dot{\varphi}\delta\varphi(\widetilde{N} - \varphi\widetilde{T} + k(\widetilde{N}^2 - \widetilde{T}^2) + 4k\varphi\widetilde{N}\widetilde{T}) + EJ\dot{\varphi}'\delta\varphi' \} ds \end{aligned}$$

5. The finite element

The internal stress variables $\tilde{\boldsymbol{\sigma}} \equiv (\widetilde{N}, \widetilde{T})$, constant on each beam element, have a natural discrete representation. However by devel-

oping the integral expressions of the strain energy variations, it can be demonstrated that the displacement fields $(u[s], w[s])$ contribute only through the discrete values $(u_j - u_i, w_j - w_i)$ where (u_i, w_i, u_j, w_j) are the relative nodal displacements. Therefore, to obtain a discrete representation of the mixed problem, only the discrete representation of the rotation field $\varphi[s]$ is needed. For this purpose we assume a classical quadratic polynomial as interpolation function, which is the solution of the Timoshenko–beam linear problem that takes into account the shear effect. In terms of *natural* variables (Argyris et al., 1977, 1979) defined by

$$e := \frac{u_j - u_i}{l}, \quad \phi_r := \frac{w_j - w_i}{l}, \quad \phi_s := \frac{\varphi_i - \varphi_j}{2}, \quad \phi_e := \frac{1}{1+\beta}\left[\frac{\varphi_i + \varphi_j}{2} - \phi_r\right]$$

where $\beta = \frac{12EJ}{GAl^2}$, the function $\varphi[s]$ then has the following expression

$$\varphi[s] = \phi_r + (1 - 2\frac{s}{l})\phi_s + (1 + \beta - 6\frac{s}{l} + 6\frac{s^2}{l})\phi_e$$

By using a *co-rotational* approach, the beam is referred to a reference system (x, z) which is rigidly connected to the deformed actual configuration, with the x axis along the straight line joining the nodal beam positions (see Fig. 2). This allows us to break down the total displacement fields of the beam into the sum of two components, the first a rigid rotation from the initial undeformed configuration to the co-rotational one, the second a pure deformation described and represented in the co-rotational reference system:

$$\mathbf{u}[s] = \mathbf{u}^r[s] + \mathbf{u}^e[s], \quad con\ \mathbf{u}^r[s] \equiv (u^r[s], w^r[s], \varphi^r),$$
$$\varphi^r = \arctan\left(\frac{\bar{w}_j - \bar{w}_i}{l_n + \bar{u}_j - \bar{u}_i}\right)$$

As the first displacement component $\mathbf{u}^r[s]$ is a rigid rotation, the co-rotational approach filters its effects in the expression of the strain energy and of its variations, now evaluated only in the second component displacement $\mathbf{u}^e[s]$. As the geometrical nonlinear effect is almost nearly totally connected to the rigid component, it means that the geometric nonlinear terms only partially affect the strain energy and its variations. This enables us to simplify some geometric nonlinear terms in their expressions as shown in Eq. (3) in the previous section. In addition, the rotation field $\varphi[s]$ is now referred to the co-rotational reference and can be minimized simply by a finer FEM discretization grid.

Discrete expressions of the strain energy variations were finally obtained by observing that in the the co-rotational reference system the following relations are valid

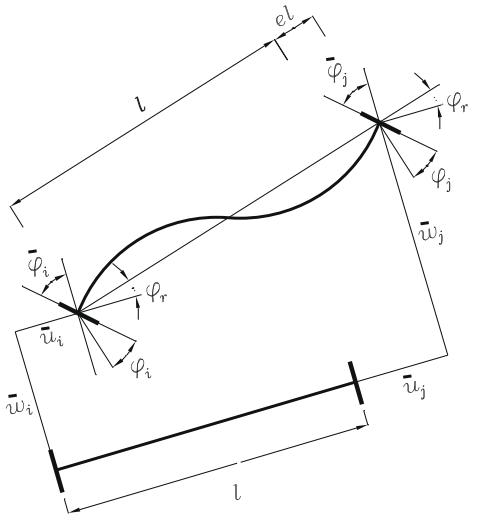

Fig. 2. The beam element in a corotational description.

$$w_i = w_j = 0, \ \ \phi_r = 0$$

5.1. The first strain energy variation (the elastic internal force vector)

Shown below is the discrete expression of the first strain energy variation:

$$\begin{aligned}\Phi'\delta r = {} & \delta e\widetilde{N}l + \delta\phi_r((\widetilde{N}+n)l\beta\phi_e - k\widetilde{N}\widetilde{T}l) \\ & + \delta\phi_s\left(\frac{1}{3}(\widetilde{N}+n)l\phi_s + 4\frac{EJ}{l}\phi_s\right) \\ & + \delta\phi_e\left((\widetilde{N}+n)\left(\frac{1}{5}+\beta^2\right)l\phi_e - (1+k\widetilde{N})\beta\widetilde{T}l + 12\frac{EJ}{l}\phi_e\right) \\ & + \delta\widetilde{N}\left(el - \frac{\widetilde{N}l}{EA} - k\widetilde{T}l\beta\phi_e\right) + \delta\widetilde{T}\left(-\frac{\widetilde{T}l}{GA} - (1+k\widetilde{N})l\beta\phi_e\right) \end{aligned} \quad (4)$$

with

$$n = k(\widetilde{N}^2 - \widetilde{T}^2) \quad (5)$$

This defines the elastic internal force vector $\mathbf{S}_e$ of the beam element on the base of the following equivalence relation:

$$\Phi'\delta r := \mathbf{S}_e^t \delta\mathbf{r_e}$$

where the vector $\delta\mathbf{r_e}$ represents variations of all the discrete kinematical $(e, \phi_r, \phi_s, \phi_e)$ and statical $(\widetilde{N}, \widetilde{T})$ parameters of the generic beam element, i.e.

$$\delta\mathbf{r}_e := [\delta e, \delta\phi_r, \delta\phi_s, \delta\phi_e, \delta\widetilde{N}, \delta\widetilde{T}]^t = [\delta\epsilon^t, \delta\tilde{\sigma}^t]^t$$

The elastic internal force vector

$$\mathbf{S}_e := [S_e, S_{\phi_r}, S_{\phi_s}, S_{\phi_e}, S_{\widetilde{N}}, S_{\widetilde{T}}]^t = [\mathbf{S}_u^t, \mathbf{S}_\sigma^t]^t \quad (6)$$

consists of the following components:

$$\begin{aligned} S_e &= \widetilde{N}l \\ S_{\phi_r} &= (\widetilde{N}+n)l\beta\phi_e - k\widetilde{N}\widetilde{T}l \\ S_{\phi_s} &= \frac{1}{3}(\widetilde{N}+n)l\phi_s + 4\frac{EJ}{l}\phi_s \\ S_{\phi_e} &= (\widetilde{N}+n)\left(\frac{1}{5}+\beta^2\right)l\phi_e - (1+k\widetilde{N})\beta\widetilde{T}l + 12\frac{EJ}{l}\phi_e \\ S_{\widetilde{N}} &= el - \frac{\widetilde{N}l}{EA} - k\widetilde{T}l\beta\phi_e \\ S_{\widetilde{T}} &= -\frac{\widetilde{T}l}{GA} - (1+k\widetilde{N})l\beta\phi_e \end{aligned}$$

5.2. The second strain energy variation (the mixed elastic tangent stiffness matrix)

The discrete expression of the second strain energy variation defines the mixed local stiffness matrix $\mathbf{K}_e^m$ on the base of the following equivalence relation

$$\Phi''\dot{r}\delta r := \dot{\mathbf{r}}_e^t \mathbf{K}_e^m \delta\mathbf{r}_e$$

The components are:

$$[\mathbf{K}_e^m] \equiv \begin{bmatrix} \mathbf{K}_{\sigma\sigma} & \mathbf{K}_{\sigma u} \\ \mathbf{K}_{u\sigma} & \mathbf{K}_{uu} \end{bmatrix} = \left[\begin{array}{cccc|cc} . & . & . & . & K_{\widetilde{N}e} & . \\ . & K_{\phi_s\phi_s} & K_{\phi_s\phi_e} & K_{\phi_r\phi_s} & K_{\widetilde{N}\phi_s} & K_{\widetilde{T}\phi_s} \\ . & K_{\phi_s\phi_e} & K_{\phi_e\phi_e} & K_{\phi_r\phi_e} & K_{\widetilde{N}\phi_e} & K_{\widetilde{T}\phi_e} \\ . & K_{\phi_r\phi_s} & K_{\phi_r\phi_e} & K_{\phi_r\phi_r} & K_{\widetilde{N}\phi_r} & K_{\widetilde{T}\phi_r} \\ \hline K_{\widetilde{N}e} & K_{\widetilde{N}\phi_s} & K_{\widetilde{N}\phi_e} & K_{\widetilde{N}\phi_r} & K_{\widetilde{N}\widetilde{N}} & K_{\widetilde{N}\widetilde{T}} \\ . & K_{\widetilde{T}\phi_s} & K_{\widetilde{T}\phi_e} & K_{\widetilde{T}\phi_r} & K_{\widetilde{N}\widetilde{T}} & K_{\widetilde{T}\widetilde{T}} \end{array}\right] \quad (7)$$

with

$$
\begin{aligned}
K_{\widetilde{N}\widetilde{N}} &= -\frac{l}{EA}\\
K_{\widetilde{N}\widetilde{T}} &= -k\beta l\phi_e\\
K_{\widetilde{N}e} &= l\\
K_{\widetilde{N}\phi_s} &= \frac{1}{3}(1+2k\widetilde{N})l\phi_s\\
K_{\widetilde{N}\phi_e} &= -k\beta\widetilde{T}l+\left(\frac{1}{5}+\beta^2\right)(1+2k\widetilde{N})l\phi_e\\
K_{\widetilde{N}\phi_r} &= -\widetilde{T}kl+(1+2k\widetilde{N})\beta l\phi_e\\
K_{\widetilde{T}\widetilde{T}} &= -\frac{l}{GA}\\
K_{\widetilde{T}\phi_e} &= -l\beta(1+k\widetilde{N})-\left(\frac{1}{5}+\beta^2\right)2k\widetilde{T}l\phi_e\\
K_{\widetilde{T}\phi_s} &= -\frac{2}{3}k\widetilde{T}l\phi_s\\
K_{\widetilde{T}\phi_r} &= -\widetilde{N}kl-2k\widetilde{T}l\beta\phi_e\\
K_{\phi_s\phi_s} &= 4\frac{EJ}{l}+\frac{1}{3}(\widetilde{N}+n)l+\left(\frac{2}{15}+\frac{\beta}{3}\right)(-1+4k\widetilde{N})\widetilde{T}l\phi_e
\end{aligned}
$$

$$
\begin{aligned}
K_{\phi_s\phi_e} &= \left(\frac{2}{15}+\frac{\beta}{3}\right)(-1+4k\widetilde{N})\widetilde{T}l\phi_s\\
K_{\phi_s\phi_r} &= \frac{1}{3}(-1+4k\widetilde{N})\widetilde{T}l\phi_s\\
K_{\phi_e\phi_e} &= 12\frac{EJ}{l}+\left(\frac{1}{5}+\beta^2\right)(\widetilde{N}+n)l+\left(\frac{2}{35}+\frac{3}{5}\beta+\beta^3\right)(-1+4k\widetilde{N})\widetilde{T}l\phi_e\\
K_{\phi_r\phi_e} &= (\widetilde{N}+n)l\beta+(-1+4k\widetilde{N})\left(\frac{1}{5}+\beta^2\right)\widetilde{T}l\phi_e\\
K_{\phi_r\phi_r} &= (\widetilde{N}+n)l+(-1+4kN)\beta\widetilde{T}l\phi_e
\end{aligned}
$$

6. The path-following strategy

In a mixed FEM approach, the state variables $\mathbf{q}$ of the structure are expressed by the nodal displacements $\mathbf{d}$ and by stress element parameters $\mathbf{s}$. For loads that increase by a λ parameter $\mathbf{p}[\lambda]=\lambda\hat{\mathbf{p}}$, the behavior of the structure describes a curve in the space $(\mathbf{d},\mathbf{s},\lambda)$ represented in implicit form using a generic scalar parameter ξ (the curvilinear abscissa)

$$\mathbf{d}[\xi],\quad \mathbf{s}[\xi],\quad \lambda[\xi] \tag{8}$$

Referring to $\mathbf{S}_d[\mathbf{d},\mathbf{s}]$ and $\mathbf{S}_s[\mathbf{d},\mathbf{s}]$ as the internal elastic response in terms of nodal displacements and stress components respectively, assembled on the basis of the relative components (6) at the local level of each beam, the *points* of the curve (8) are solutions of the nonlinear equations system

$$\lambda\hat{\mathbf{p}}-\mathbf{S}_d[\mathbf{d},\mathbf{s}]=0 \tag{9a}$$

$$\mathbf{S}_s[\mathbf{d},\mathbf{s}]=0 \tag{9b}$$

$$g[\mathbf{d},\mathbf{s},\lambda]=\xi \tag{9c}$$

where Eq. (9a) expresses the nodal equilibrium conditions of the problem, Eq. (9b) the internal kinematic compatibility conditions inside the elements and Eq. (9c) the scalar relation that defines the curvilinear abscissa ξ.

The path-following numerical algorithm for the reconstruction of the curve (8) is based on a succession of steps each defined by

- a *predictor phase*, i.e. an extrapolation starting from a known point

$$\mathbf{d}_1=\mathbf{d}_o+\Delta\mathbf{d},\quad \mathbf{s}_1=\mathbf{s}_o+\Delta\mathbf{s},\quad \lambda_1=\lambda_o+\Delta\lambda$$

- and a *corrector phase*, i.e. an iterative sequence converging to a new point of the curve

$$\mathbf{d}_{j+1}=\mathbf{d}_j+\dot{\mathbf{d}},\quad \mathbf{s}_{j+1}=\mathbf{s}_j+\dot{\mathbf{s}},\quad \lambda_{j+1}=\lambda_j+\dot{\lambda}$$

It should be noted that the iterative sequence is regulated by the jacobian matrix $\mathbf{J}$ of the system (9). The problem can be expressed in the following form

$$\overbrace{\begin{bmatrix}\frac{\partial\mathbf{S}_d}{\partial\mathbf{d}} & \frac{\partial\mathbf{S}_d}{\partial\mathbf{s}}\\ \frac{\partial\mathbf{S}_s}{\partial\mathbf{d}} & \frac{\partial\mathbf{S}_s}{\partial\mathbf{s}}\end{bmatrix}}^{\mathbf{K}^m}\begin{bmatrix}\dot{\mathbf{d}}\\ \dot{\mathbf{s}}\end{bmatrix}=\begin{bmatrix}(\lambda_j+\dot{\lambda})\hat{\mathbf{p}}-\mathbf{S}_d^j\\ -\mathbf{S}_s^j\end{bmatrix} \tag{10a}$$

$$\Delta\mathbf{u}^t\mathbf{M}\dot{\mathbf{u}}+\mu\Delta\lambda\dot{\lambda}=0 \tag{10b}$$

in terms of tangential matrix of the mixed problem $\mathbf{K}^m$ assembled on the basis of the local matrices $\mathbf{K}_e^m$ of the beam elements given by (7), and suitably transforming the Eq. (9c) into the condition (10b), which constraints the corrector components $(\dot{\mathbf{d}},\dot{\lambda})$ to belong to the normal plane of the predictor components $(\Delta\mathbf{d},\Delta\lambda)$, making use of a suitable metric operator defined in terms of the quantities $(\mu,\mathbf{M})$.

It is known that the direct factorization of the mixed matrix $\mathbf{K}^m$ is not the most efficient computational strategy to solve the problem (10a). It can instead be solved in a partitioned form, through a block Gaussian elimination of the stress variables $\dot{\boldsymbol{\sigma}}$ at each beam finite element level, where the system (10) has the following localization

$$\overbrace{\begin{bmatrix}\mathbf{K}_{uu} & \mathbf{K}_{u\sigma}\\ \mathbf{K}_{\sigma u} & \mathbf{K}_{\sigma\sigma}\end{bmatrix}}^{\mathbf{K}_e^m}\begin{bmatrix}\dot{\mathbf{u}}\\ \dot{\boldsymbol{\sigma}}\end{bmatrix}=\begin{bmatrix}(\lambda_j+\dot{\lambda})\hat{\mathbf{p}}^e-\mathbf{S}_u^j\\ -\mathbf{S}_\sigma^j\end{bmatrix} \tag{11}$$

$\hat{\mathbf{p}}^e$ being the (unknown) part of the load $\hat{\mathbf{p}}$ associated with the element and using the definitions of Eqs. (6) and (7). The Gauss elimination of the stress variable $\dot{\boldsymbol{\sigma}}$

$$\dot{\boldsymbol{\sigma}}=-\mathbf{K}_{\sigma\sigma}^{-1}\mathbf{K}_{\sigma u}\dot{\mathbf{u}}-\mathbf{K}_{\sigma\sigma}^{-1}\mathbf{S}_\sigma^j$$

transforms the problem (11) into

$$\underbrace{(\mathbf{K}_{uu}-\mathbf{K}_{u\sigma}\mathbf{K}_{\sigma\sigma}^{-1}\mathbf{K}_{\sigma u})}_{\mathbf{K}_e^c}\dot{\mathbf{u}}=(\lambda_j+\dot{\lambda})\hat{\mathbf{p}}^e-\mathbf{S}_u^j+\mathbf{K}_{\sigma\sigma}^{-1}\mathbf{S}_\sigma^j$$

now controlled by the local tangential stiffness matrix $\mathbf{K}_e^c$ of the compatible formulation. Using standard procedures to assemble the terms at the global level ($\mathbf{A}_e$ is the matrix of kinematical compatibility of the element)

$$\mathbf{K}^c=\sum_e\mathbf{A}_e^t\mathbf{K}_e^c\mathbf{A}_e\ \cdot\ \mathbf{S}_d^j=\sum_e\mathbf{A}_e^t\mathbf{S}_u^j\ \cdot\ \Delta\mathbf{S}_{ds}^j=\sum_e\mathbf{A}_e^t\mathbf{K}_{\sigma\sigma}^{-1}\mathbf{S}_\sigma^j$$

transforms the problems (10a) to the condensed form

$$\mathbf{K}^c\dot{\mathbf{d}}=(\lambda_j+\dot{\lambda})\hat{\mathbf{p}}-\mathbf{S}_d^j+\Delta\mathbf{S}_{ds}^j$$

which is almost identical to that of the compatible formulation ($\mathbf{K}^c$ is the usual tangential stiffness matrix of the structure), enriched however by an additional contribute $\Delta\mathbf{S}_{ds}^j$ which expresses the influence of the condensed stress variables. From a computational point of view, the problem now has a much simpler solution which can be obtained by a standard factorization procedure of the matrix $\mathbf{K}^c$.

7. Numerical results

The proposed finite beam element in a mixed path-following formulation was then checked in the light of the numerical results. The aim was to verify the accuracy and the performance of the strategy, comparing the results with other available solutions, and at the same time to analyse the influence of shear deformation

effects. The analysis was performed varying the finite element discretization and for several values of the stiffness ratios $k = \frac{EAl^2}{EJ}$ and $s = \frac{GA}{EA}$.

7.1. Cantilever beam

In the first example, a cantilever beam was studied under two different load conditions. The first is a condition of pure bending with a concentrated moment M applied to its free end. This is a test to verify the accuracy of the suggested FEM strategy in reproducing a very large rotation of the beam. In fact the beam deforms, in accordance to Euler formula, into involved circular shapes and an exact analytical solution of the equilibrium path can be easily obtained (see Ibrahimbegovic, 1997). As can be seen in Fig. 3 where the load parameter $\frac{Ml}{EJ}$ is plotted vs. the lateral end displacement parameter $\frac{w}{l}$, accurate results are obtained with a discretization of just two finite elements.

The second condition deals with a concentrated force P applied to the free end of the beam. In this case, to explore the influence of the shear deformability, several tests are performed varying the ratio $s = \frac{GA}{EA}$. The results are plotted in Fig. 4 and show again that only few finite elements are needed to reproduce accurate values (with no exact analytical solutions available, the comparison is made with a discretization of 100 finite elements). This is essentially true for relatively large values of the ratio s, while some discrepancy can be observed for low values of s and large values of the displacement parameter $\frac{w}{l}$.

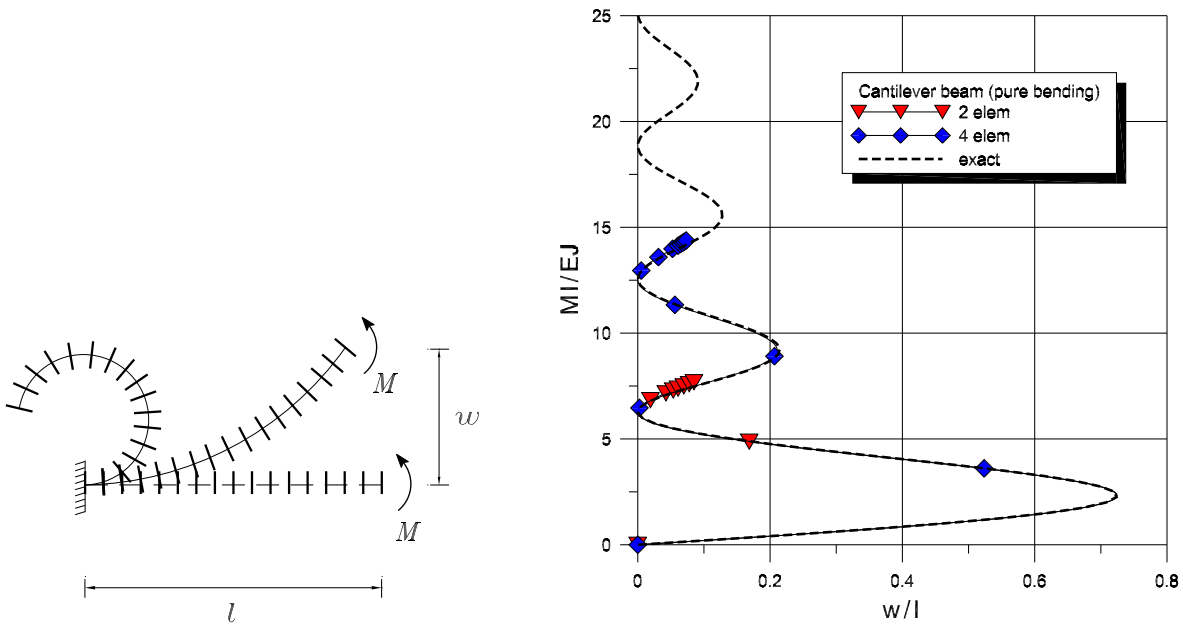

Fig. 3. Cantilever beam in pure bending (example 1).

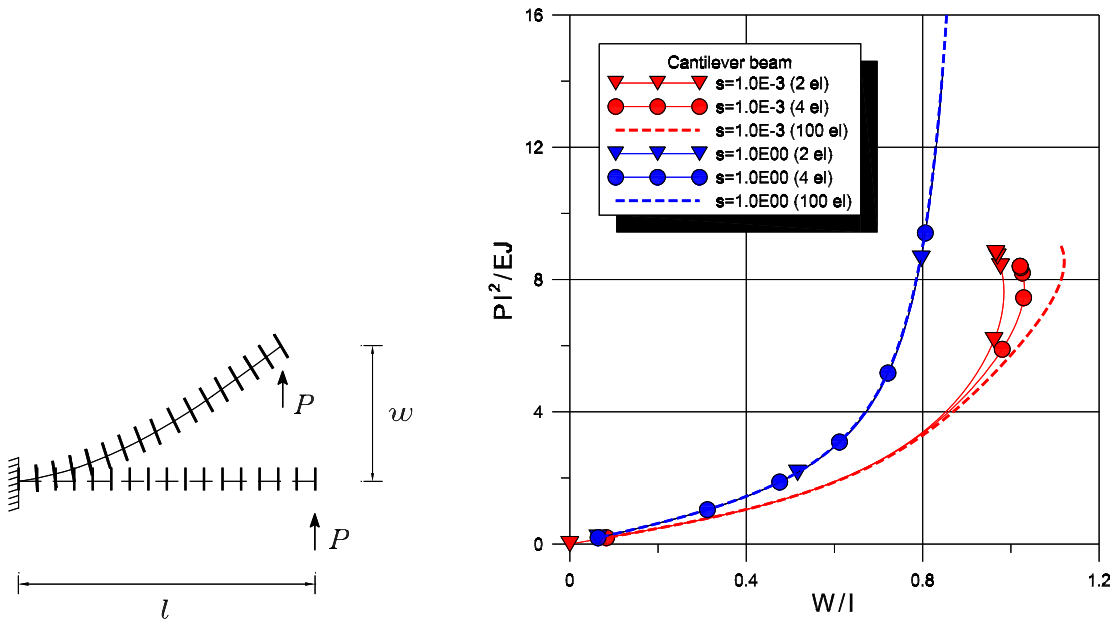

Fig. 4. Cantilever beam in shear and bending condition (example 2).

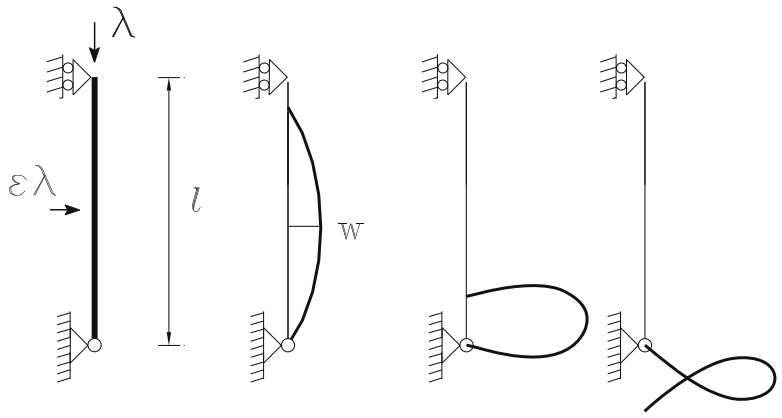

Fig. 5. Euler Beam (example 3).

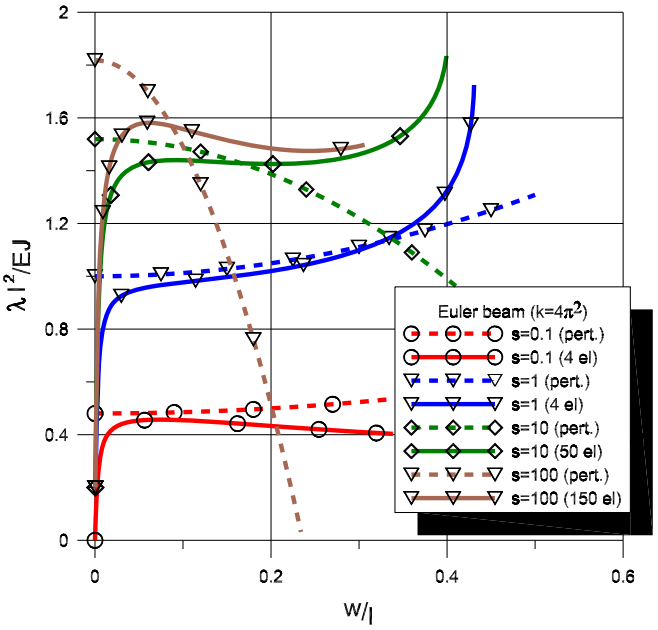

Fig. 6. Load vs. displacement of Euler beam $\left(\frac{EAl^2}{EJ} = 4\pi^2\right)$.

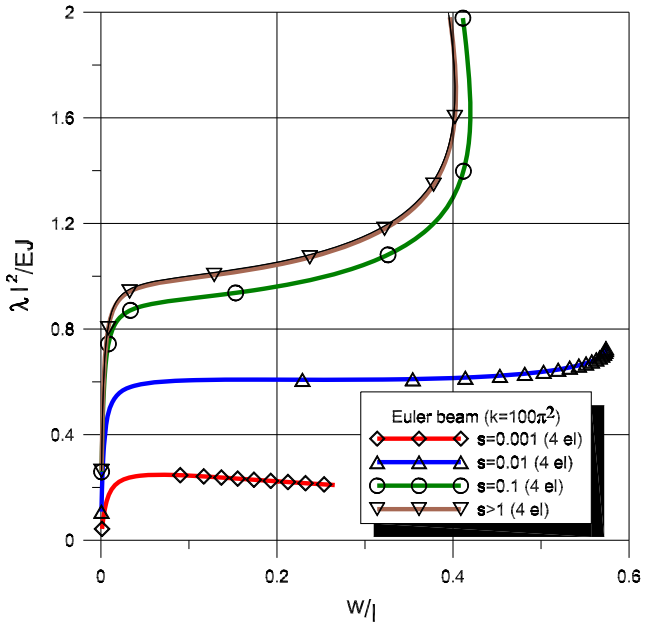

Fig. 7. Load vs. displacement of Euler beam $\left(\frac{EAl^2}{EJ} = 100\pi^2\right)$.

7.2. Euler beam

The example shown in Fig. 5 is a Euler beam, analyzed with a transversal load 0.01λ, where λ is the axial compression load. The tests were performed for two different values of the ratio $k = \frac{EAl^2}{EJ}$ and for several values of the ratio $s = \frac{GA}{EA}$, while at the same time varying the number n of discretization elements of the beam. The results are represented in Figs. 6 and 7 in terms of load parameter $\frac{\lambda l^2}{EJ}$ vs. central transversal displacement parameter $\frac{w}{l}$ of the equilibrium paths.

For all the tests of the case $\frac{EAl^2}{EJ} = 4\pi^2$ (see Fig. 6), the solution of the perfect initial post-buckling behavior of the perturbation approach obtained analytically in Salerno and Lanzo (1997) and Lanzo (2004) is reported in dashed lines. In this case and for $s = 1$ the solutions correspond exactly to those obtained using the model by Garcea et al. (1998). Furthermore, only a few finite elements (n = 2–4) were needed to obtain accurate results. The perturbative approximated curve predicts this solution quite well, both in qualitative (with a stable post-buckling path) and in quantitative terms. With a lower value of the ratio parameter s, i.e. when shear stiffness is noticeably lower than the axial stiffness, the load value at which lateral buckling phenomena occur are greatly reduced. Again, this can be accurately predicted with only a few elements. This case exhibits a decreasing post-buckling behavior, which is far from the stable post-buckling behavior predicted by an approximated perturbation approach. Higher values of the ratio parameter s increase the buckling load. More specifically, $s = 10$ and $s = 100$ tests initially exhibit an unstable post-buckling path (correctly predicted by the perturbative approach) but subsequently show an increased load carrying capacity (ascending path) which cannot be reproduced by the approximated perturbation approach. In this case, however, accurate solutions require a large number of discretization elements ($n = 50$ for $s = 1$ and $n = 150$ for $s = 100$).

For all the tests of the case $\frac{EAl^2}{EJ} = 100\pi^2$ (see Fig. 7), the solutions are accurately obtained with only a few elements. The shear effects are negligible for higher values of the ratio parameter s (for $s > 1$ the solution substantially coincides with that for $s = 1$). The level of influence is sensitive for lower values of s, as can be observed in the equilibrium paths traced in Fig. 7.

7.3. Roorda's frame

This example is the classical Roorda's frame (Roorda, 1965) with a load λ of eccentricity $e = l/1000$ (see Fig. 8). Tests were

performed for two different values of the ratio $k = \frac{EAl^2}{EJ}$ and for several values of the ratio $s = \frac{GA}{EA}$. Accurate solutions in terms of equilibrium paths were obtained with a discretization of just $4 + 2$ finite elements. The results are represented in Fig. 9 plotting the ratio $\frac{\lambda l^2}{EJ}$ vs. the rotation φ of the central node. For $k = 1.0 \times 10^3$ an influence of the ratio parameter s can be observed for values $s < 10$, while the curves are practically identical for $s > 10$. This influence is negligible throughout for $k = 1.0 \times 10^7$.

7.4. A deep arch

The clamped-hinged deep arch of Fig. 10 has already been the subject of extensive study. The solution represented here was obtained using 20 finite elements and varying the ratio $s = \frac{GA}{EA}$. The shear influence can be observed only for small values of the parameter s ($s = 1/1000$), while for higher values of s the results largely coincide with those produced in Garcea et al. (1998) and Kouhia and Mikkola (1989), here obtained for the specific case $s = 1$.

7.5. A rigidly jointed truss

The rigidly jointed truss of Fig. 11 was examined in Salerno and Lanzo (1997); Garcea et al., 1998 (the results there reported are affected by errors in the graphical representation). The solution in

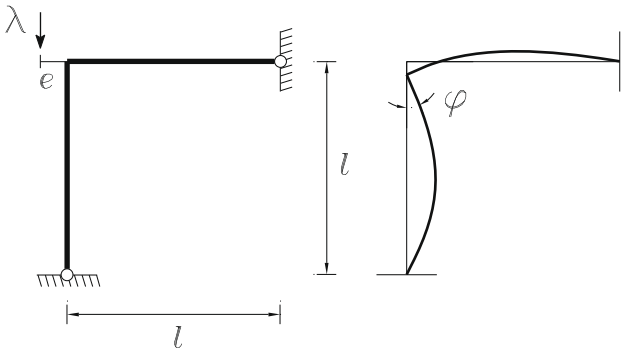

Fig. 8. Roorda's frame (example 4).

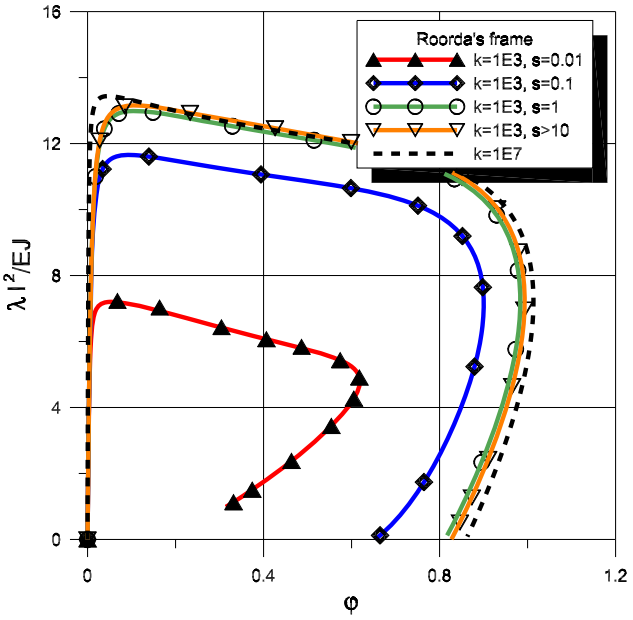

Fig. 9. Load vs. displacement of Roorda's frame.

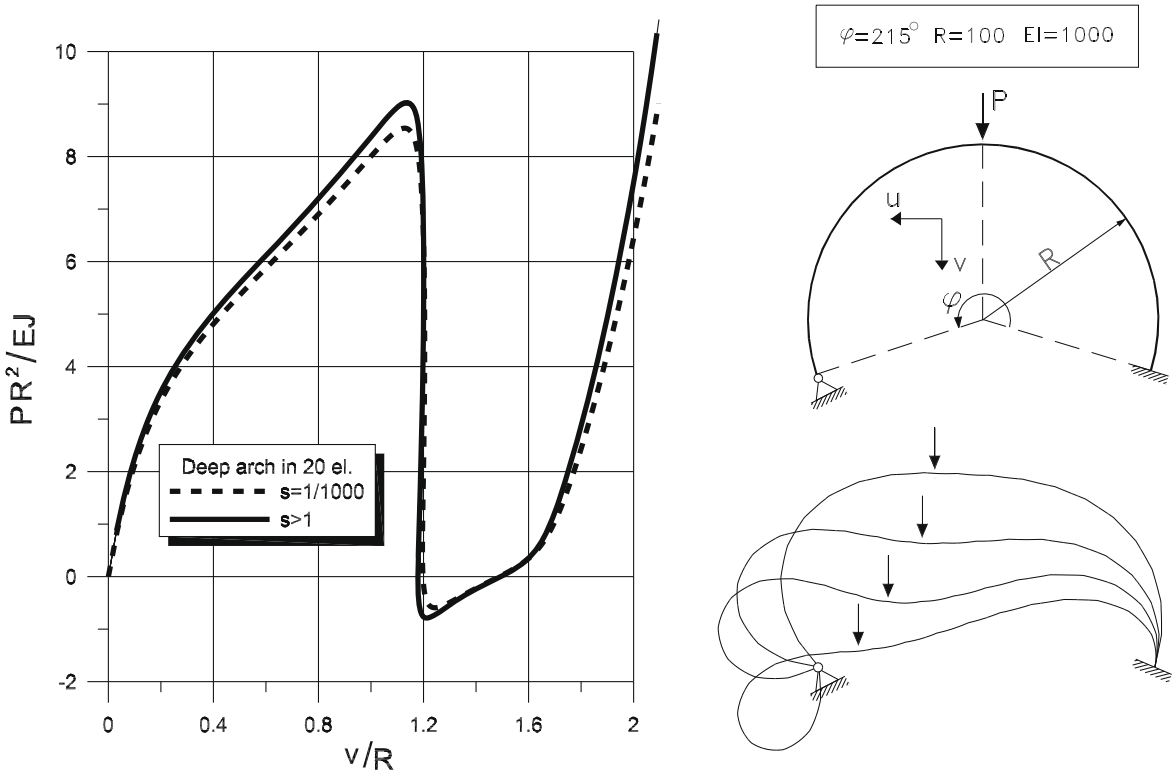

Fig. 10. Deep arch (example 5).

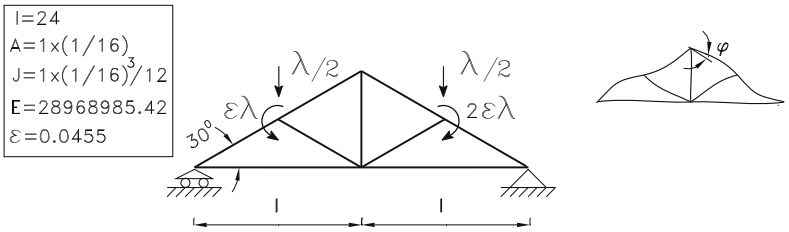

Fig. 11. Rigidly jointed truss (example 6).

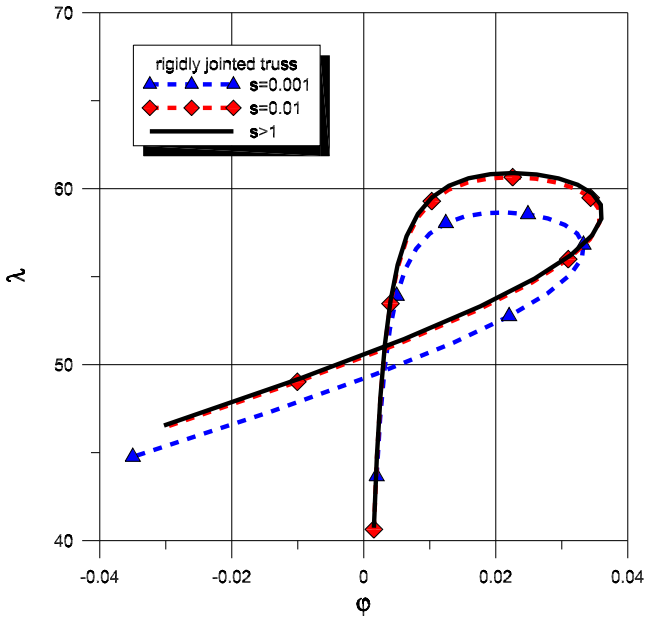

Fig. 12. Load vs. displacement of example 6.

the present paper uses a discretization of four finite elements for each beam of the truss. As with the previous example, the results represented in Fig. 12 also exhibit a shear factor influence only for small values of the parameter $s = \frac{GA}{EA}$, while for values $s \geqslant 1$ this influence is negligible.

8. Conclusions

This paper presented a mixed implementation of the Riks path-following strategy for the analysis of elastic plane frames, which effectively takes into account their flexural, axial and shear deformation contributions. The mixed strategy uses a step control defined both in terms of displacements and internal stress (axial N and transversal T) components, in addition to the load parameter. The finite element model is based on a Cosserat beam and an accurate discrete interpolation (exact in terms of stress components). At any step of the strategy, a partitioned numerical solution is implemented, using a block Gaussian elimination of the stress variables at each beam finite element level, which leads at a global level to a condensed problem almost identical to that of the usual displacement-based compatible formulation. Some numerical tests are presented in order to prove the effectiveness of the strategy and the influence of shear contribution on known classical examples.

References

Antman, S.S., 1977. Bifurcation problems for nonlinearly elastic structures. In: Rabinowitz, P.H. (Ed.), Applications of Bifurcation Theory. Academic Press, New York.

Antman, S.S., 1995. Nonlinear Problems of Elasticity. Springer-Verlag, New York.

Argyris, J.H., Dunne, P.C., Scharpf, D.W., 1977. On large displacement–small strain analysis of structures with rotational degrees of freedom. Comput. Methods Appl. Mech. Eng. 12, 97–124.

Argyris, J.H. et al., 1979. Finite element method – the natural approach. Comput. Methods Appl. Mech. Eng. (17/18), 1–106.

Garcea, G., Trunfio, G.A., Casciaro, R., 1998. Mixed formulation and locking in path-following nonlinear analysis. Comput. Methods Appl. Mech. Eng. 165, 247–272.

Ibrahimbegovic, A., 1997. On the choice of finite rotation parameters. Comput. Methods Appl. Mech. Eng. 149, 49–71.

Kouhia, R., Mikkola, M., 1989. Tracing the equilibrium path beyond simple critical points. Int. J. Numer. Methods Eng. 28, 2923–2941.

Lanzo, A.D. 1994. La trave come continuo monodimensionale dotato di struttura euclidea: studio di un modello (in Italian), In: Report 158, Dipartimento di Strutture, Universitá della Calabria, Cosenza, Italy.

Lanzo, A.D., 2004. On elastic beam models for stability analysis of multilayered rubber bearings. Int. J. Solids Struct. 41 (20), 5733–5757.

Pignataro, M., Di Carlo, A., Casciaro, R., 1982. On nonlinear beam model from the point of view of computational post-buckling analysis. Int. J. Solids Struct. 18 (4), 327–347.

Riks, E., 1972. The application of Newton's method to the problem of elastic stability. J. Appl. Mech. 39, 1060–1066.

Riks, E., 1979. An incremental approach to the solution of snapping and buckling problems. Int. J. Solids Struct. 15, 529–551.

Roorda, J., 1965. Stability of structures with small imperfections. J. Eng. Mech. Div. ASCE (EMI) 91, 87–106.

Rubin, M.B., 2000. Cosserat Theories: Shells, Rods and Points. Kluwer Academic Publishers, London.

Salerno, G., Lanzo, A.D., 1997. A nonlinear beam finite element for the post-buckling analysis of plane frames by Koiter's perturbation approach. Comput. Methods Appl. Mech. Eng. 146, 325–349.